NJC

ROYAL SOCIETY OF CHEMISTRY

PAPER

View Article Online
View Journal | View Issue

Cite this: *New J. Chem.*, 2024, **48**, 12919

Synthesis and spectroscopic properties of carotenoid bis-phenylhydrazone astaxanthin: extending conjugation to a C=N group†

Emrah Özcan, *[a] Gürkan Keşan,[a] Pavel Chábera, [b] Radek Litvín[c] and Tomáš Polívka [a]

Received 15th May 2024,
Accepted 30th June 2024

DOI: 10.1039/d4nj02282c

rsc.li/njc

We report on the synthesis and detailed spectroscopic characterization of bis-phenylhydrazone astaxanthin (**BPH-Asx**), a derivative of astaxanthin (**Asx**), in which the conjugated carbonyl group of **Asx** is replaced by a conjugated C=N bond. **BPH-Asx** was successfully synthesized and characterized using various spectroscopic techniques, revealing subtle changes in absorption spectra and significant alterations in excited-state dynamics compared to **Asx**. The results reveal a shortened S_1 lifetime, 1.4 ps for **BPH-Asx** compared to 5 ps for **Asx**, indicating a significant impact on its excited-state dynamics. Since no polarity-induced effect was observed for **BPH-Asx**, the changes induced by the conjugated C=N group are due to prolongation of effective conjugation. Moreover, the identification of a distinctive S* signal with a 3 ps lifetime in **BPH-Asx** underscores the relation between effective conjugation and presence of the S* signal that is not detected in **Asx**.

Introduction

Carotenoids are a class of natural pigments with extraordinary photoprotective[1] and light-harvesting[2,3] abilities in biological systems. Moreover, their rich excited-state dynamics[4] as well as capacity to engage in various functions, such as quenching of singlet-excited states of chlorophylls,[5–8] chlorophyll triplets,[9,10] and antioxidation achieved by scavenging singlet oxygen or other reactive oxygen species,[11–16] emphasize their importance in both biology and chemistry. Due to their important roles in light-induced processes, photophysical and photochemical properties of carotenoids have been frequently studied; however, owing to the complicated excited-state structure and dynamics, gaps in understanding the carotenoid photophysics still remain.

According to the basic description of the excited states of all carotenoids, two states are highlighted: strongly absorbing S_2 state and lower-lying S_1 state, to which a one-photon transition from the ground state (S_0) is forbidden due to the multiply-excited character.[17] Thus, the lowest energy one-photon transition from the ground state occurs to the S_2 state, which relaxes to the S_1 state whose properties are readily monitored *via* its characteristic S_1–S_n band in transient absorption spectra.[18,19] This general picture is valid for all carotenoids and their conjugated C=C bond chain structures, common in all carotenoids, primarily determine their photophysical properties.[17]

Beyond this three-state model (S_0, S_1 and S_2), other states have been identified. In keto-carotenoids, featuring a conjugated C=O bond in their structure, an intramolecular charge transfer (ICT) state coupled to the dark S_1 state is stabilized in a polar environment, resulting in a state commonly referred as the S_1/ICT.[20,21] The presence of the ICT state is easily detected by characteristic bands in the transient absorption spectrum. The ICT-like transition is red-shifted from the S_1–S_n band for most keto-carotenoids. The amplitude ratio between the S_1–S_n and ICT-like bands serves as a measure of degree of charge transfer character of the coupled S_1/ICT state.[20,21] Numerous investigations have demonstrated that the degree of charge transfer character is proportional to solvent polarity but the conjugation length and position of the conjugated keto group are also crucial factors. The ICT signal increases for short keto-carotenoids having a single keto group positioned asymmetrically while the charge transfer nature of the S_1/ICT state is minimized for long ones with two keto groups positioned symmetrically.[20,22,23] This is for example the case of astaxanthin (**Asx**), one of the widely studied keto-carotenoids, which has two symmetric conjugated keto (C=O) groups at the

[a] *Department of Physics, Faculty of Science, University of South Bohemia, Branišovská 1760, České Budějovice 370 05, Czech Republic. E-mail: ozcane00@prf.jcu.cz*
[b] *Division of Chemical Physics, Department of Chemistry, Lund University, Box 142, Lund SE-221 00, Sweden*
[c] *Department of Chemistry, Faculty of Science, University of South Bohemia, Branišovská 1760, České Budějovice 370 05, Czech Republic*

† Electronic supplementary information (ESI) available. See DOI: https://doi.org/10.1039/d4nj02282c

terminal rings, resulting in only a weak ICT signal detected in a broad range of solvents.[24–26]

Another state known as S* has been identified in carotenoids with long conjugation. The S* signal is typically demonstrated as a distinct blue shoulder at the S_1–S_n band, and its lifetime is longer than that of the S_1 state.[27] The origin of the S* signal is still a matter of debate. The first detection of the S* signal assigned it to a hot ground state,[28] but this assignment was later challenged and the S* signal was instead attributed to a separate excited state.[27] Since then, numerous studies favoring either ground state[29,30] or excited state[31,32] hypothesis have been reported. Yet, it seems that both hot ground state and excited state contribute to the S* signal, with particular contribution depending on conjugation length: while for short conjugation ($N < 11$) the excited state contribution dominates, a hot ground state is the key source of the S* signal for long carotenoids.[33]

Since excited state dynamics of carotenoids depends on the structure of the conjugated system, synthetic carotenoids with various modifications of the conjugated chain helped to understand some aspects of carotenoid photophysics. These modifications often focused on synthesis of carotenoids with a conjugation length longer than that of natural carotenoids. Such approach, involving a synthesis of β-carotene analogs with 15 or even 19 C=C bonds (in contrast to 11 in natural β-carotene), led to the first observation of the S* signal.[28] Series of synthetic carotenoids with varying conjugation lengths later helped to understand excited-state dynamics of β-carotene,[34] zeaxanthin[35] or keto-carotenoids peridinin[36] and fucoxanthin.[37]

Besides synthesis of carotenoid series with the same structure but different conjugation lengths, chemical modifications of carotenoids have also targeted various functional groups involved in conjugation in order to test their role in excited-state dynamics. To this end, alterations of the allene group of peridinin[38] or fucoxanthin[39] were used to test the effect of the allene group on ICT state of these keto-carotenoids. Similarly, symmetry of peridinin was modified by 'moving' the lactone ring along the main conjugated chain.[40] Many synthetic carotenoids have been introduced in the past few decades including those having non-natural atoms such as sulfur, nitrogen, or phosphorus in their structure.[41] Yet, excited state dynamics of these carotenoids has not been studied, apart from two exceptions featuring nitrogen atoms in their structure. First, ultrafast dynamics of all-*trans*-7′,7′-dicyano-7′-apo-β-carotene,[42] demonstrating strong effect of the cyano groups on excited state lifetime. Second, astaxanthin (**Asx**) esterified by the amino acid lysine, synthesized to make **Asx** water soluble, was subjected to ultrafast transient absorption spectroscopy.[43]

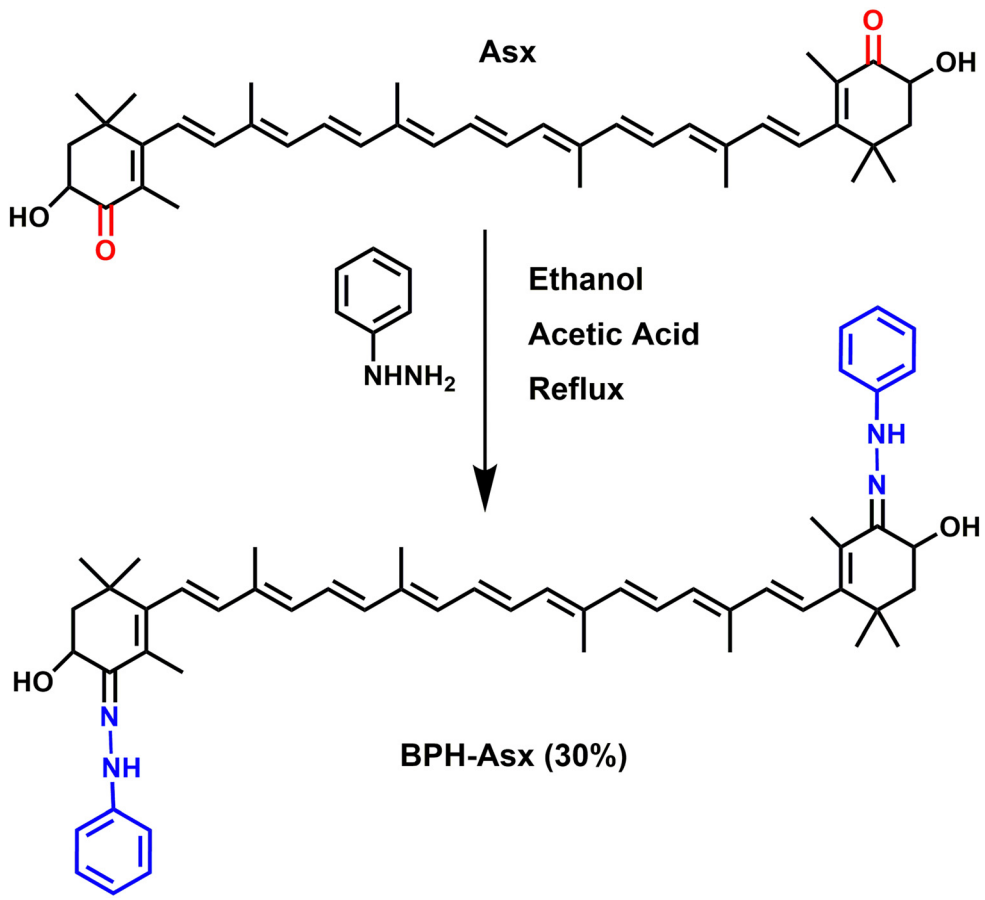

Scheme 1 Synthetic pathway of bis-phenylhydrazone astaxanthin (**BPH-Asx**).

Asx is a subject of chemical modification also in this study. It has two oxygen atoms on each cyclohexene rings in the form of a keto (C═O) and hydroxyl (C–OH) group. These groups at terminal rings offer a possibility of chemical/structural modification of **Asx**, synthesizing novel carotenoids.[44–46] Since such modification of **Asx**, especially that modifying the keto group, is expected to change the photophysical properties, it is an ideal tool to explore features of excited states of the **Asx**. More specifically, by the synthesis of novel carotenoids (Scheme 1), we can obtain astaxanthin whose conjugated C═O group, the expected generator of the ICT state, is modified to some other functional group. Such modification could figure out whether a carbonyl group is needed for observation of spectroscopic features related to the ICT state.

Here, we report on synthesis of a novel astaxanthin derivative named bis-phenylhydrazone astaxanthin (**BPH-Asx**) which instead of conjugated C═O group has C═N bond in conjugation. We have conducted a detailed study of its photophysical properties that were investigated by ultrafast time-resolved transient absorption spectroscopy. The data showed that Asx could be successfully modified, resulting in stable **BPH-Asx**, which has significantly different spectroscopic properties compared to **Asx**.

Experimental section

Materials and methods

Astaxanthin (Sigma Aldrich, ≥97%, HPLC), phenylhydrazine (Merck, ≥97%, for synthesis), ethanol (Penta, ≥97%, GC), glacial acetic acid (Lachner, 99.8 G.R.), acetonitrile (ACN, Fluka, ≥99.9%, HPLC), benzene (Fluka, ≥99.5%, GC), methanol (Merck, ≥99.9%, HPLC), and dichloromethane (DCM, Merck, ≥99.9%, GC) were used as obtained without further purification. Reactions were monitored by thin layer chromatography using Merck TLC Silica gel 60 with DCM/methanol (1/1, v/v) as the eluent. MALDI-TOF mass spectra were acquired in linear modes with average of 50 shots on a Bruker Daltonics Microflex mass spectrometer equipped with a nitrogen UV-Laser operating at 337 nm. ESI-MS detection was conducted on a Bruker QqTOF compact instrument operated using Compass Control 4.0 software (Bruker Daltonics, Germany). Compass DataAnalysis 4.4 (Build 200.55.2969) (Bruker Daltonics, Germany) software was used for data processing. NMR spectra (^{1}H and ^{13}C NMR) were recorded for all compounds in $CDCI_3$ by a Varian INOVA 500 MHz spectrometer using TMS as internal reference. High-performance liquid chromatography (HPLC) was performed using a Waters Alliance HPLC system with a PDA 2998 detector (Waters, USA). The compounds were injected in methanol and separated on a reverse phase Nova-Pak C18 column (3.9 × 300 mm, 4 μm, silica-based, end-capped; Waters, USA) using a linear gradient elution. A tertiary solvent system used was as follows:[47] solvent A (80 : 20 methanol: 0.5 M ammonium acetate (aq., pH 7.2 v/v)), solvent B (90 : 10 acetonitrile : water), solvent C (100% ethyl acetate). The flow rate was 1 mL min^{-1}. Absorption spectra of the samples were measured in a 10-mm path length quartz cuvette using UV-vis spectrometer (Shimadzu UV-2600). Fluorescence spectra were measured in 3 × 3 mm quartz cells using Horiba Fluorolog-3 spectrometer, using Xe arc lamp, double monochromators and a photomultiplier detector at right angle detection geometry.

Synthesis of bis-phenylhydrazone astaxanthin (BPH-Asx)

Astaxanthin 10 mg (0.017 mmol), excess phenylhydrazine 7.34 mg (0.068 mmol) and a few drops of glacial acetic acid in ethanol (25 mL) were heated at reflux overnight. The resulting precipitate was filtered and washed with cold ethanol (100 mL). As the TLC of the solid part was clear, no further separation was applied. **BPH-Asx** was obtained as an orange-red color powder (4 mg, 30%). MALDI TOF (*m/z*) (Fig. S1, ESI†) calc. 776.50, found: 776.998 $[M + H]^+$; ESI-MS (Fig. S1, ESI†): $C_{52}H_{63}N_4O_2$ $[M^+]$ calculated 775.4945, found: 775.4936 *m/z*. ^{1}H NMR (Fig. S2, ESI;† 500 MHz, $CDCl_3$) δ 9.61 (s, 2H, NH, j), 7.24 (4H, Ar–CH, h), 7.12 (d, J = 8.0 Hz, 4H, Ar–CH, h), 6.84 (t, J = 7.6 Hz, 2H, Ar–CH, g), 6.66 (t, J = 14.9 Hz, 4H, alkene H, f), 6.42 (d, J = 14.9 Hz, 2H, alkene H, f), 6.29–6.22 (m, 8H, alkene H, f), 5.30 (s, 2H, CH, e) 4.83 (s, 2H, OH, d), 2.10 (s, 4H, CH_2, c), 1.99–2.00 (s, 12H, CH_3, b), 1.13–1.25 (s, 18H, CH_3, a) ppm. ^{13}C NMR (Fig. S3, ESI;† 125 MHz, $CDCl_3$) δ 150.3, 138.4, 137.5, 136.7, 135.1, 130.3, 129.6, 129.1, 128.5, 128.3, 126.8, 124.3, 114.4, 68.5, 53.8, 30.8, 30.2, 27.5, 26.4, 21.9 ppm. FT-IR (Fig. S4, ESI;† ATR, cm^{-1}) ν = 3300 cm^{-1} (NH), ν = 1750 cm^{-1} (C═N), ν = 1251 cm^{-1} (C–N), ν = 1500–1600 cm^{-1} (C═O).

Transient absorption spectroscopy

Transient absorption (TA) spectroscopy was measured using an in-house build setup, based on a Solstice ACE (Spectra Physics) laser amplifier system that produces ∼60 fs pulses at a central wavelength of 796 nm at 4 kHz repetition rate. The amplifier output is divided into two parts that each pump an optical parametric amplifier (TOPAS-C, Light Conversion). One generates the pump beam while the other produces a NIR beam (1360 nm) that is focused onto a 3 mm CaF_2 crystal to generate a supercontinuum probe beam. The delay between pump and probe pulses is introduced by a computer-controlled delay stage (Aerotech, 10 ns) placed in the probe beam path. After supercontinuum generation the probe pulses are split into two parts: the former being focused to ∼100 μm spot size and overlapping with the pump pulse in the sample volume, and the latter serving as a reference. After passing the sample the probe beam is collimated again and relayed onto the entrance aperture of a prism spectrograph. Both beams are then dispersed onto a double photodiode array, each holding 512 elements (Pascher Instruments). The intensity of excitation pulses was set to 230 μW, yielding excitation density of 6.5 × 10^{13} photons per pulse per cm^2. Mutual polarization between pump and probe beams was set to the magic angle (54.7°) by placing a Berek compensator in the pump beam. Time-resolution of the setup after dispersion correction is estimated to be ≤100 fs. The measured samples, placed in a 1-mm pathlength optical cuvette, were translated after each scan to avoid photodegradation. To check for stability of each sample steady-state

absorption spectra were measured before and after experiments.

Data analysis

The resulting spectro-temporal data sets were analyzed by a global fitting software (CarpetView, Light Conversion, Lithuania). It was assumed that the excited system evolves irreversibly and sequentially to visualize the excited-state dynamics. Each component of the sequential scheme illustrates an individual excited-state species, and the spectral profile of each species is called the evolution-associated difference spectrum (EADS). The same software was used for chirp-correction of the spectra.

Results

Synthesis and structural characterization

BPH-Asx was successfully prepared by using the procedure described in literature.[48] The synthesis procedure of **BPH-Asx** is detailed in Scheme 1. The **BPH-Asx** was synthesized by the condensation reaction of commercially available **Asx** and phenylhydrazine in ethanol and in the presence of a catalytic amount of glacial acetic acid. After reaction reflux overnight, solid **BPH-Asx** was obtained with a reasonable yield (30%) by just washing with cold EtOH/MeOH to remove excess/unreacted phenylhydrazine. The **BPH-Asx** obtained without further purification appeared as an orange-red solid. The successful condensation of **Asx** with phenylhydrazine to produce the desired target compound, **BPH-Asx**, was confirmed by using various spectroscopic techniques.

The molecular ion peak of the **BPH-Asx** was determined by the MALDI-TOF mass spectrometer as 776.998 *m/z*, which is in good agreement with the predicted structure, and further confirmed by ESI-MS (Fig. S1, ESI†). The novel **BHP-Asx** structure was further supported by comparing its ^{1}H NMR spectroscopic data with that of commercially available **Asx** (Fig. S2, ESI†). The proposed chemical structure for **BPH-Asx** were confirmed by analysis of both aromatic and aliphatic protons. Specifically, in the case of **BPH-Asx**, additional resonances of aromatic benzene protons at 7.24 and 7.12 (10H, g and h), along with a new resonance of NH (2H, j) proton at 9.61 ppm, were identified. The presence of these additional characteristic protons strongly supports the structural confirmation of **BPH-Asx**. In the ^{13}C NMR spectrum, the aromatic carbons of the **BHP-Asx** were marked between 150.3 and 114.4 and the aliphatic carbons signals were seen between the 68.5 and 21.9 ppm regions of the spectra (Fig. S3, ESI†). FT-IR spectroscopy is a useful and effective method for investigating structural changes in molecules and we compare the FT-IR spectra of **BPH-Asx** and **Asx** in Fig. S4 (ESI†). In the FT-IR spectrum of **BPH-Asx**, distinctive peaks were observed at 3300 cm^{-1} corresponding to the NH stretching vibrations, 1750 cm^{-1} indicate of the C=N stretching vibrations, and 1251 cm^{-1} were attributed to the C–N stretching vibrations. Notably, in comparison to astaxanthin, **BPH-Asx** exhibited these new characteristic peaks and the absence of the strong peak at 1660 cm^{-1} associated with the C=O stretching vibrations. These spectral structural differences between **BPH-Asx** and **Asx** further confirm the proposed structure and alterations of functional groups.

Asx and its modified derivative **BPH-Asx** were analyzed by HPLC for further characterization (Fig. S5, ESI†). The chromatogram of **Asx** consists of a single broad peak at 11.1 min, identified as all-*trans* **Asx**.[49] The chromatogram of **BPH-Asx** exhibits five peaks, occurring at longer retention times

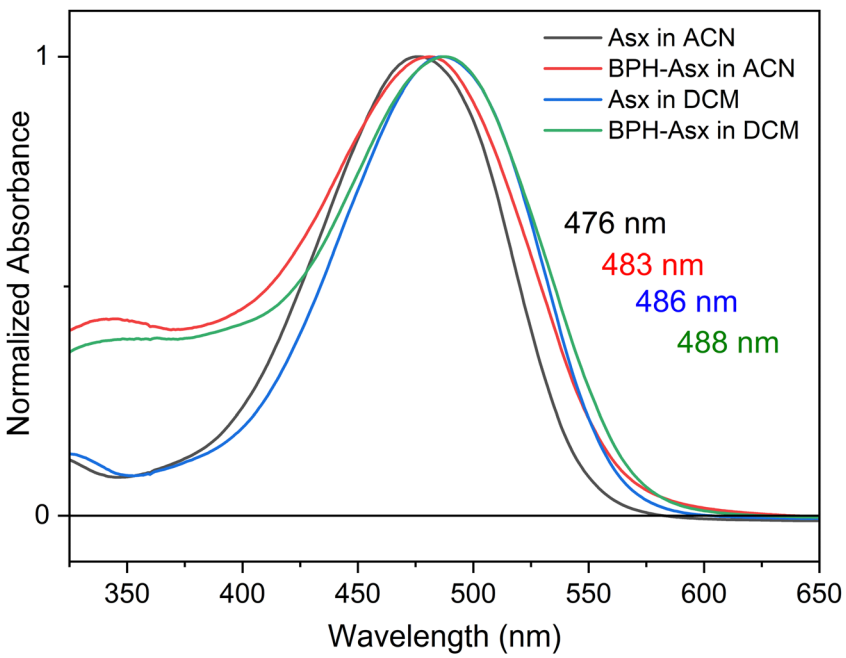

Fig. 1 Steady state absorption spectra of **Asx** and **BPH-Asx** in acetonitrile and dichloromethane.

compared to **Asx**. The highest peak at 12.9 minutes (81%) was identified as **BPH-Asx**. Two minor peaks at 13.9 minutes (6%), 14.1 minutes (6%) showed absorbance bands around 380 nm (Fig. S6, ESI†) and likely correspond to *cis*-isomers of **BPH-Asx**.[49] Presence of small amount of some unidentified **Asx**-related species was indicated by a minor peak at 12.2 minutes (3%). The last minor peak at 15.6 minutes (4%) showed significantly red-shifted absorbance (Fig. S6, ESI†) indicating significantly longer effective conjugation in the ground state. This could be caused by the *s-trans* configuration of the terminal rings making the whole conjugation linear including the two C═N groups (Scheme 1).

Steady-state and transient absorption spectroscopy

Absorption spectra of **Asx** and **BPH-Asx** in acetonitrile (ACN) and dichloromethane (DCM) are depicted in Fig. 1. The absorption maximum of **Asx** is at 476 nm in ACN with a single broad peak, reflecting the S_0–S_2 transition, in agreement with previous reports on **Asx** in this solvent.[25] The absorption maximum of **Asx** red shifts with increasing solvent polarizability, peaking at 486 nm in DCM. For **BPH-Asx**, absorption spectra in both solvents exhibit a small red shift compared to **Asx**: the absorption maxima are at 483 and 488 nm in ACN and DCM, respectively. A slightly broader distribution of the S_0–S_2 transition energies is observed for **BPH-Asx**, but overall, the comparison of absorption spectra suggests that the transition dipole moment associated with the S_0–S_2 transition undergoes only modest changes upon change from **Asx** to **BPH-Asx**. The properties of the S_0–S_2 transition are further confirmed by fluorescence spectra shown in Fig. S7 (ESI†). The weak fluorescence originates from the S_2 state in agreement with data reported on **Asx** earlier.[50] The solvent induced red-shift of fluorescence spectrum is larger for **Asx** than for **BPH-Asx**, mirroring the behavior of absorption spectra.

Transient absorption spectra at different time delays following excitation are shown in Fig. 2. The excitation wavelength was at 500 nm for **Asx** and **BPH-Asx** in both solvents, intended to excite the molecules just below the maximum of the S_0–S_2 transition. The data provide characteristic carotenoid transient absorption spectra, comprising ground state bleaching and excited state absorption (ESA) attributed to the S_1–S_n transition for both **Asx** and **BPH-Asx**. The S_1–S_n band of **Asx** in ACN, peaking at 629 nm, is consistent with previous studies,[25] fully forming within the first picosecond. In DCM, the S_1–S_n peak shifts to 642 nm (Fig. 2a and b). In addition to the dominant S_1–S_n transition, a weak band in the 700–800 nm spectral region indicates the presence of an ICT state. The ICT signal is weak for **Asx** due to its symmetrically positioned conjugated C═O groups that minimize the charge transfer character of the coupled S_1/ICT state as has been also demonstrated for other carbonyl carotenoids.[22] The 800–900 nm spectral region exhibits an additional ESA band at early delays (0.15 ps), which is linked to the ESA from the initially excited S_2 state.[51]

Although the general features observed in the transient absorption spectra of both carotenoids look similar, the modification of the conjugated chain from **Asx** to **BPH-Asx** induces

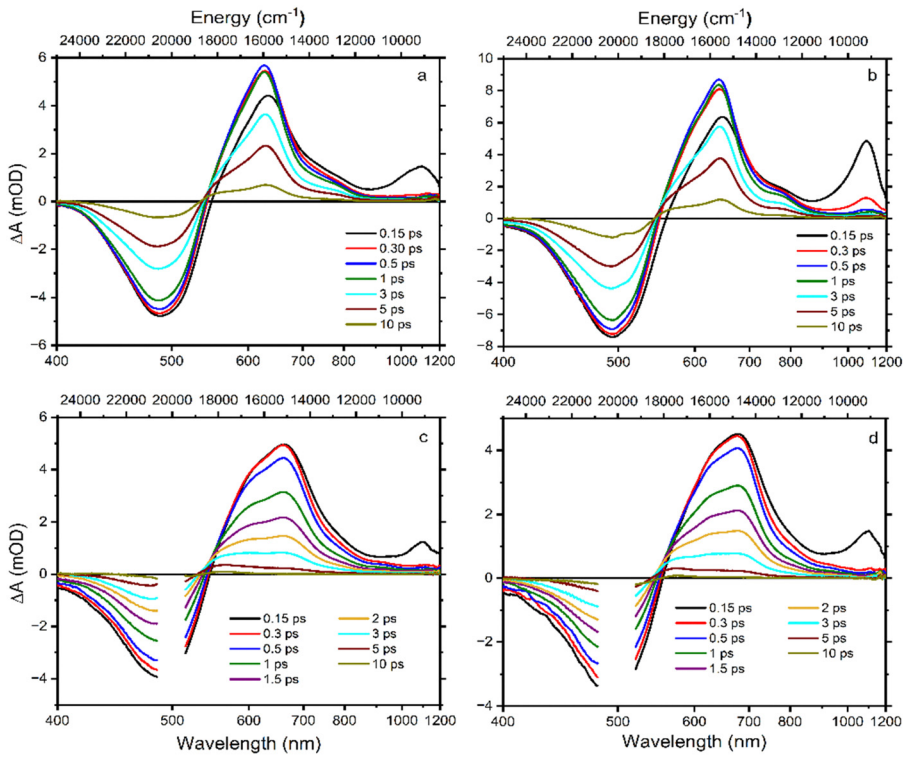

Fig. 2 Transient absorption spectra of **Asx** in ACN (a), **Asx** in DCM (b), **BPH-Asx** in ACN (c), and **BPH-Asx** in DCM (d). The delay times after 500 nm excitation are indicated in each panel. The color-coding is the same in all panels.

some changes in the transient absorption spectra. As expected, both the ground state bleaching and S_1–S_n ESA exhibit a red shift, reflecting the observed difference in the ground state absorption spectra. The S_1–S_n bands of **BPH-Asx** have maxima at 642 nm and 681 nm in ACN and DCM, respectively (Fig. 2c and d). Besides the changes in the S_1–S_n band, the ESA signal associated with the S_2–S_n band of **BPH-Asx** at 0.15 ps after excitation did not show any shift but had less amplitude compared to **Asx**. The signal associated with the ICT state is much less pronounced in **BPH-Asx** as it nearly disappears in both solvents. However, this can be partly due to a broader S_1–S_n band of **BPH-Asx**, resulting in a weak ICT band hidden under the dominant S_1–S_n transition, which extends to 800 nm for **BPH-Asx**.

To visualize these changes, Fig. 3a compares normalized transient absorption spectra at 1 ps after excitation of both compounds in both solvents. The decrease in the magnitude of the ICT band, along with the red shift observed when going from **Asx** to **BPH-Asx**, is evident. Excited state dynamics was monitored by kinetics measured at the maximum of the S_1–S_n band (Fig. 3b). The decay is significantly faster for **BPH-Asx** compared to **Asx**, while there is no change for both compounds with respect to solvent polarity.

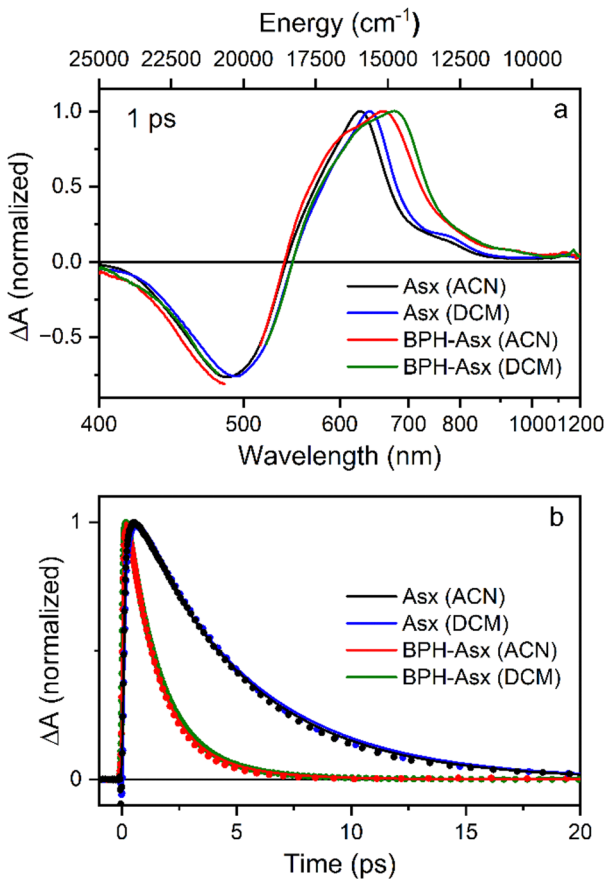

Fig. 3 (a) Normalized transient absorption spectra of **Asx** and **BPH-Asx** in both solvents. The spectra were measured at 1 ps after excitation at 500 nm for all compounds/solvents. (b) Normalized kinetics measured at the S_1–S_n maximum for each sample. The solid lines represent fits obtained from global fitting analysis.

Excited state lifetimes were determined using a global fitting analysis, and the results are summarized in Fig. 4. For both compounds, three decay components are sufficient to obtain good fits. The first EADS for **Asx** in both solvents show features typical of the excited **Asx** S_2 state, and its lifetime is at sub-100 fs time scale, reaching the limit of our time resolution. The second EADS has already typical features of the S_1–S_n band except the increased amplitude at the low energy side of the band, which is characteristic of a hot S_1/ICT state.[52]

Decay of the hot S_1/ICT state occurs within a few hundred femtoseconds, differing slightly between ACN (350 fs) and DCM (240 fs) and yields EADS of the relaxed S_1/ICT state. This EADS exhibits the characteristic profile of the relaxed S_1/ICT state and decays with a time constant of 4.85 ps (ACN) and 5 ps (DCM). This pattern of the excited state dynamics of **Asx** in ACN agrees with the results obtained earlier.[25,52]

For **BPH-Asx**, three decay components provide a good fit, but the individual EADS differ from those obtained for **Asx**. The first EADS with sub-100 fs lifetime clearly contains features associated with both S_2 state (the ESA signal peaking around 1100 nm) and the hot S_1/ICT state. This implies that S_2 and hot S_1/ICT decays are both very short and occur on a comparable time scale, preventing separation of their contributions with our time resolution. Then, the second EADS corresponds to the relaxed S_1/ICT state, which has a lifetime of 1.3 ps in ACN and 1.4 ps in DCM. In contrast to **Asx**, however, global fitting of **BPH-Asx** reveals EADS with a lifetime longer than the S_1/ICT state. This EADS (blue in Fig. 4c and d) has a spectral shape characteristic of an S* signal, which is typically indicated by a distinct blue shoulder at the S_1–S_n band, with a longer lifetime compared to the S_1 state.[27] Here, the S* EADS has a lifetime of 3 ps.

To further visualize the difference, we compared kinetics measured at the peak maxima of S_1/ICT and S* bands for both **Asx** and **BPH-Asx** (Fig. 5). The kinetics clearly demonstrate that while the kinetics of **Asx** are identical, **BPH-Asx** exhibits a slower decay of the S* signal compared to the S_1/ICT decay in both ACN and DCM, as expected.

Discussion

A straightforward chemical reaction of **Asx** with phenylhydrazine and acetic acid in ethanol produced stable **BPH-Asx** with ~30% yield, demonstrating a successful synthesis of a first carotenoid with a conjugated C=N group. Formally, structure of the conjugated system of **BPH-Asx** is the same as for **Asx** except the C=O groups of **Asx**, located symmetrically at both terminal rings, are replaced by C=N groups in **BPH-Asx**. This allows to study the effect of replacement of the C=O group by the C=N group on spectroscopic properties directly. The presence of keto-groups in **Asx** generates a featureless absorption spectrum, most likely due to enhanced conformational disorder in the ground state produced by a broad distribution

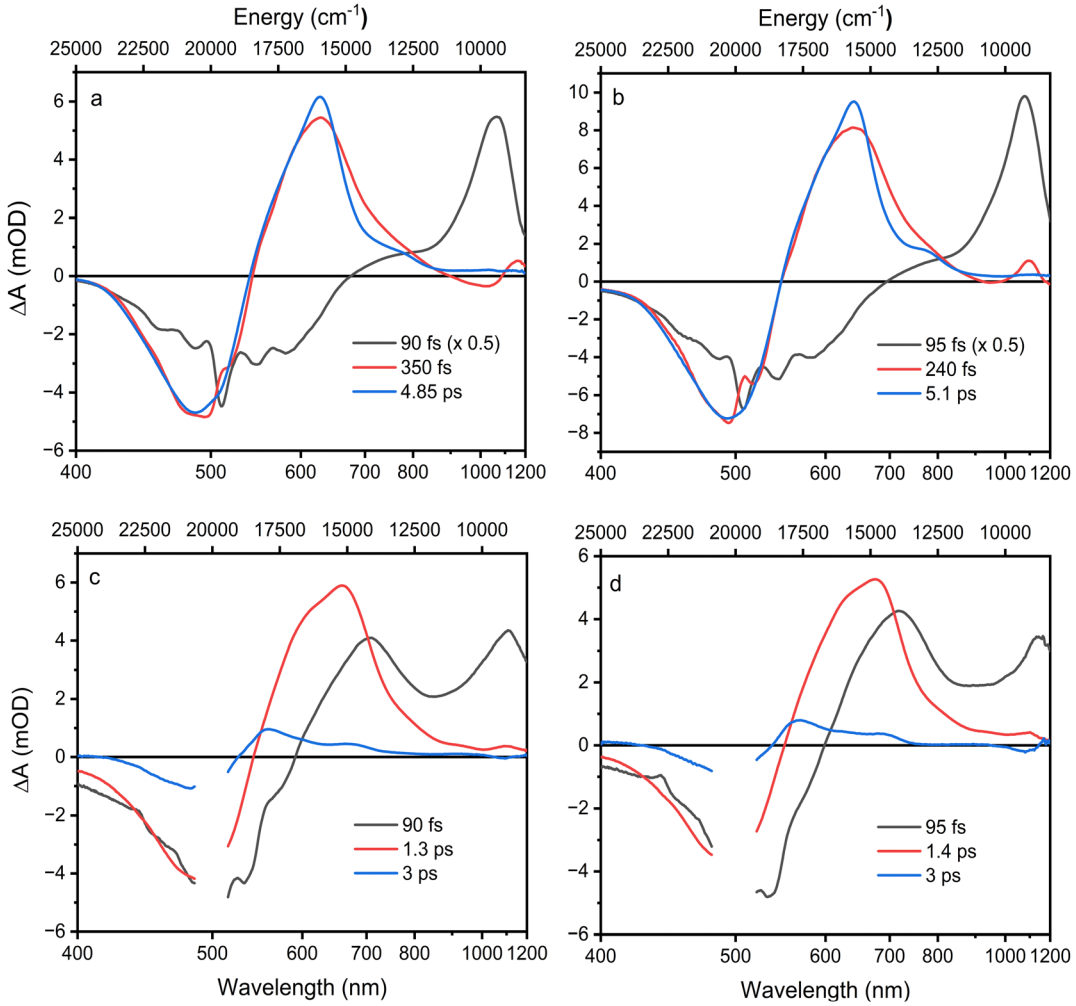

Fig. 4 EADS obtained from global fitting of **Asx** in ACN (a), **Asx** in DCM (b), **BPH-Asx** in ACN (c), and **BPH-Asx** in DCM (d).

of end ring torsions. The relevant carotenoid without these conjugated keto-groups (zeaxanthin) has absorption spectrum with clearly resolved vibrational bands, proving the importance of the keto-groups in forming the featureless absorption spectrum. The same apparently happens when the keto groups are replaced by the C═N group: the overall shape of the main absorption band is very similar, though the absorption spectrum of **BPH-Asx** is slightly broader, suggesting further enhancement of conformational disorder. Furthermore, absorption maximum of **BPH-Asx** is red-shifted by a few nanometers which is the first indication of changes of spectroscopic properties induced by the conjugated C═N group. Solvent polarity has minimal effect on absorption spectrum of **BPH-Asx**, which is in striking contrast to the dicyano-apocarotene, another carotenoid featuring nitrogen atoms in conjugation.[42]

While the changes in absorption spectra are rather subtle, more pronounced changes occur in excited state dynamics. The red shift of **BPH-Asx** is enhanced in transient absorption spectra reflecting the S_1–S_n band, but the most significant effect of the conjugated C═N group is on the S_1/ICT lifetime. Even though the ICT band amplitude is not enhanced in **BPH-Asx**, the S_1/ICT lifetime drops from ∼5 ps (**Asx**) to ∼1.4 ps (**BPH-Asx**). Since the S_1/ICT lifetimes are essentially identical in DCM and ACN (Fig. 4), the shortening can hardly be associated with solvent polarity. To verify this, we have measured additional data for both carotenoids in non-polar benzene (Fig. S8 and S9, ESI†). The data clearly show that further decrease of solvent polarity does not have any effect on spectroscopic properties. The S_1/ICT lifetime is the same in benzene and ACN, proving that the observed shortening of the S_1/ICT lifetime is not due to solvent polarity, but it rather indicates a prolongation of effective conjugation length for **BPH-Asx**.

The effective conjugation length can be determined by comparison of the S_1/ICT lifetime with that of carotenes.[53] The S_1/ICT lifetime of **Asx**, ∼5 ps, is comparable to that of the linear lycopene with N = 11. Shortening of the S_1/ICT lifetime to 1.4 ps (**BPH-Asx**) suggests effective conjugation of ∼13. This implies that the conjugated C═N groups contribute to the total conjugation length significantly more than the C═O groups. Another support for explanation of the observed changes in spectroscopic properties solely by prolongation of

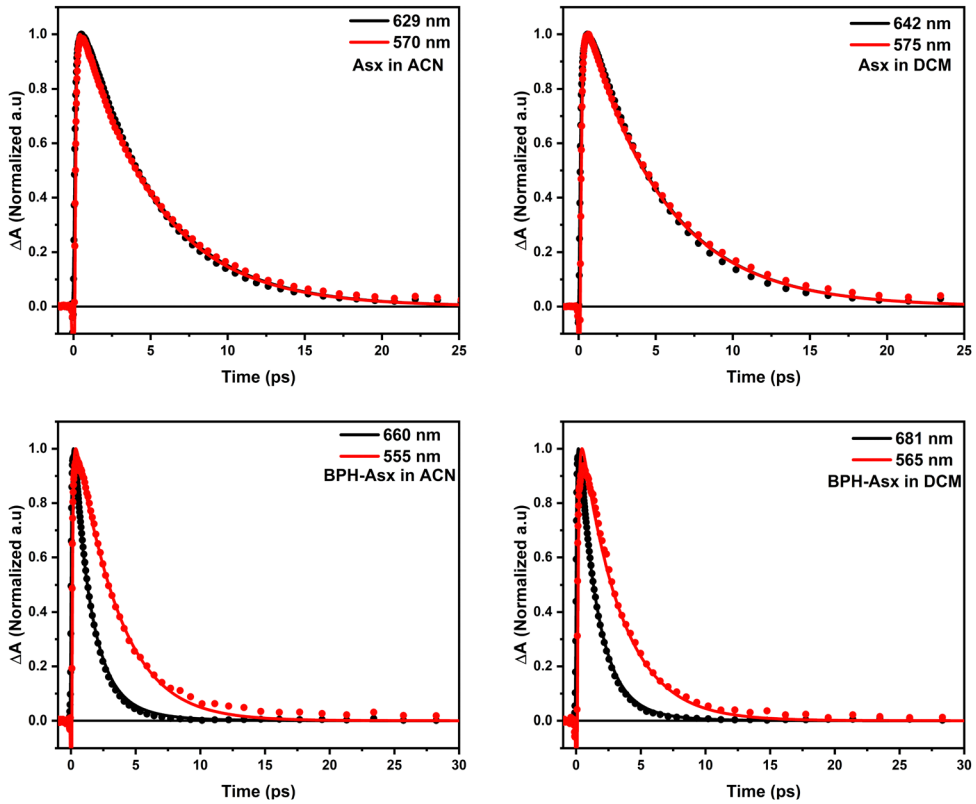

Fig. 5 Comparison of normalized kinetics measured at the S_1 (black) and S* (red) maximum bands of **Asx** and **BPH-Asx** in polar and non-polar solvents. The lines represent fits obtained from global fitting analysis.

the effective conjugation is detection of the S* signal exclusively in **BPH-Asx**. The blue shoulder (S*) of the S_1–S_n band decaying slower than the main S_1–S_n band (Fig. 5) is a feature reported exclusively for carotenoids with $N > 11$.[33] Though the origin of this signal is not completely clear, recent studies have showed that for these long carotenoids the S* signal is likely due to a hot ground state populated by fast decay of the S_1 state.[33] Thus, the distinct lifetimes of the S* and S_1/ICT signals, 3 and 1.4 ps provide further support for explanation of the differences between spectroscopic properties of **Asx** and **BPH-Asx** by prolongation of the effective conjugation.

To identify possible origin of the proposed prolongation of effective conjugation, we have examined both molecules by calculations using density functional theory. The structures were optimized using the B3LYP level of theory with 6-31g(d,p) basis set. Since the prolongation of the effective conjugation in carotenoids with conjugation extended to terminal rings is often associated with twisting of the end rings resulting in planarization of the conjugated system,[53] we have focused on dihedral angles between the terminal rings and the main conjugation chain. For the relaxed ground state structures of **Asx** and **BPH-Asx** *in vacuo* we have obtained values of -38.5° and -43.7° (see Fig. S10 for relaxed structures, ESI†). These values are close to those reported for **Asx** earlier[54] and indicate that planarization of **BPH-Asx** cannot be the reason for prolongation of the conjugation length. Thus, a different mechanism must operate here, likely related to the properties of the conjugated C=N group that is further connected to other, non-conjugated part of the phenylhydrazone group. Even though non-conjugated groups usually do not contribute to the effective conjugation length, for some keto-carotenoids, electron distribution in the excited state has been affected by non-conjugated groups, resulting in a change of excited-state properties.[55] It is likely that comparable mechanism works also here as there is only mild change (small red-shift of absorption spectrum) of spectroscopic properties in the ground state, but significant change occurs for the lowest excited state, somehow mimicking the behaviour reported in ref. 54.

Longer effective conjugation length of **BPH-Asx** and no effect of solvent polarity on its excited states is in striking contrast with another carotenoid involving a nitrogen atom in conjugated system, dicyano-apo-carotene, which exhibits a strong dependence of excited state properties on solvent polarity as its S_1 lifetime varies by an order of magnitude from 11.7 ps in 3-methylpentane to 1.9 ps in ACN.[42] This is due to a significant charge transfer character of the excited state, because dicyano-apo-carotene has two C≡N groups but both located at the same side of the molecule, generating large asymmetry in the electron distribution along the conjugated chain. **BPH-Asx** in contrast, has two C=N groups positioned symmetrically at ends of the conjugated chain, preventing asymmetry in electron distribution which is the source of polarity-induced effects on excited state dynamics.[20–23] Instead, adding two symmetric phenylhydrazone groups extends the electron distribution

along the conjugated chain, making the effective conjugation of **BPH-Asx** longer than of **Asx**.

In conclusion, we have demonstrated that the carotenoid astaxanthin can be successfully modified with organic compounds *via* a new and simple synthetic pathway, adding non-native groups to the astaxanthin conjugated system, which may provide a basis for synthesis of further non-natural carotenoids. The modification of **Asx** presented here results in significant changes of photophysical properties, opening a way to study effects that are not present in natural carotenoids. This approach may help to shed more light on complicated structure of carotenoid excited states as well as on intricate relaxation pathways involving dark excited states, eventually contributing to a deeper understanding of complex photophysical properties of carotenoids.

Author contributions

Emrah Özcan: conceptualization, investigation, data curation, formal analysis, methodology, writing – original draft, writing – review & editing. Pavel Chábera: methodology, investigation. Gürkan Keşan: methodology, investigation. Radek Litvín: conceptualization, methodology, supervision, writing – original draft, writing – review & editing. Tomáš Polívka: conceptualization, funding acquisition, writing – original draft, writing – review & editing, supervision.

Data availability

The datasets generated and/or analyzed during the current study are available from the corresponding author on reasonable request.

Conflicts of interest

There are no conflicts of interest to declare.

Acknowledgements

The research leading to these results has received funding from the Czech Science Foundation (grant 19-28323X), and LASERLAB-EUROPE (grant agreement no. 871124, European Union's Horizon 2020 research and innovation programme). EO further thanks Gebze Technical University for technical support in enabling mass spectroscopy, NMR, and FTIR measurements, and Profs Bünyemin Çoşut and İbrahim Fazıl Ş engül for their help and support. The authors thank to Petr Štěpnička and Martin Štícha from Charles University for their help with ESI-MS measurements.

References

1 K. K. Namitha and P. S. Negi, *Crit. Rev. Food Sci. Nutr.*, 2010, **50**, 728–760.
2 T. Polívka and H. A. Frank, *Acc. Chem. Res.*, 2010, **43**, 1125–1134.
3 R. Croce and H. van Amerongen, *Science*, 2020, **369**, 2058.
4 D. Zigmantas, T. Polívka, P. Persson and V. Sundström, *Chem. Phys. Rev.*, 2022, **3**, 041303.
5 A. V. Ruban, R. Berera, C. Ilioaia, I. H. van Stokkum, J. T. Kennis, A. A. Pascal, H. van Amerongen, B. Robert, P. Horton and R. van Grondelle, *Nature*, 2007, **450**, 575–578.
6 N. E. Holt, D. Zigmantas, L. Valkunas, X. P. Li, K. K. Niyogi and G. R. Fleming, *Science*, 2005, **307**, 433–436.
7 H. Staleva, J. Komenda, M. K. Shukla, V. Slouf, R. Kana, T. Polivka and R. Sobotka, *Nat. Chem. Biol.*, 2015, **11**, 287–291.
8 C. D. P. Duffy and A. V. Ruban, *J. Photochem. Photobiol., B*, 2015, **152**, 215–226.
9 T. G. Monger, R. J. Cogdell and W. W. Parson, *Biochim. Biophys. Acta*, 1976, **449**, 136–153.
10 Z. Kvíčalová, J. Alster, E. Hofmann, P. Khoroshyy, R. Litvín, D. Bína, T. Polívka and J. Pšenčík, *Biochim. Biophys. Acta, Bioenerg.*, 1857, **2016**, 341–349.
11 H. A. Frank and R. J. Cogdell, *Photochem. Photobiol.*, 1996, **63**, 257–264.
12 C. S. Foote, Y. C. Chang and R. W. Denny, *J. Am. Chem. Soc.*, 1970, **92**, 5216–5218.
13 T. W. M. Boileau, A. C. Moore and J. W. Erdman, *J. Antioxid. Act.*, 1999, 133–158.
14 S. A. R. Paiva and R. M. Russell, *J. Am. Coll. Nutr.*, 1999, **18**, 426–433.
15 N. I. Krinsky and K.-J. Yeum, *Biochem. Biophys. Res. Commun.*, 2003, **305**, 754–760.
16 M. Kobayashi and Y. Sakamoto, *Biotechnol. Lett.*, 1999, **21**, 265–269.
17 T. Polívka and V. Sundström, *Chem. Rev.*, 2004, **104**, 2021–2072.
18 T. Polívka and V. Sundström, *Chem. Phys. Lett.*, 2009, **477**, 1–11.
19 M. R. Wasielewski and L. D. Kispert, *Chem. Phys. Lett.*, 1986, **128**, 238–243.
20 H. A. Frank, J. A. Bautista, J. Josue, Z. Pendon, R. G. Hiller, F. P. Sharples, D. Gosztola and M. R. Wasielewski, *J. Phys. Chem. B*, 2000, **104**, 4569–4577.
21 D. Zigmantas, R. G. Hiller, F. P. Sharples, H. A. Frank, V. Sundstrom and T. Polivka, *Phys. Chem. Chem. Phys.*, 2004, **6**, 3009–3016.
22 M. M. Enriquez, M. Fuciman, A. M. LaFountain, N. L. Wagner, R. R. Birge and H. A. Frank, *J. Phys. Chem. B*, 2010, **114**, 12416–12426.
23 P. Chábera, M. Fuciman, P. Hříbek and T. Polívka, *Phys. Chem. Chem. Phys.*, 2009, **11**, 8795–8803.
24 E. Özcan, V. Kuznetsova, G. Keşan, M. Fuciman, R. Litvín and T. Polívka, *J. Photochem. Photobiol., A*, 2023, **441**, 114737.
25 R. P. Ilagan, R. L. Christensen, T. W. Chapp, G. N. Gibson, T. Pascher, T. Polivka and H. A. Frank, *J. Phys. Chem. A*, 2005, **109**, 3120–3127.

26 N. Christensson, T. Polivka, A. Yartsev and T. Pullerits, *Phys. Rev. B: Condens. Matter Mater. Phys.*, 2009, **79**, 245118.
27 C. C. Gradinaru, J. T. M. Kennis, E. Papagiannakis, I. H. M. van Stokkum, R. J. Cogdell, G. R. Fleming, R. A. Niederman and R. van Grondelle, *Proc. Natl. Acad. Sci. U. S. A.*, 2001, **98**, 2364.
28 P. O. Andersson and T. Gillbro, *J. Chem. Phys.*, 1995, **103**, 2509.
29 W. Wohlleben, T. Buckup, H. Hashimoto, R. J. Cogdell, J. L. Herek and M. Motzkus, *J. Phys. Chem. B*, 2004, **108**, 3320.
30 T. Lenzer, F. Ehlers, M. Scholz, R. Oswald and K. Oum, *Phys. Chem. Chem. Phys.*, 2010, **12**, 8832.
31 E. Papagiannakis, I. H. M. van Stokkum, M. Vengris, R. J. Cogdell, R. van Grondelle and D. S. Larsen, *J. Phys. Chem. B*, 2006, **110**, 5727.
32 D. M. Niedzwiedzki, J. O. Sullivan, T. Polivka, R. R. Birge and H. A. Frank, *J. Phys. Chem. B*, 2006, **110**, 22872–22885.
33 V. Balevičius, D. Abramavicius, T. Polívka, A. Galestian Pour and J. Hauer, *J. Phys. Chem. Lett.*, 2016, **7**, 3347–3352.
34 D. Kosumi, M. Fujiwara, R. Fujii, R. J. Cogdell, H. Hashimoto and M. Yoshizawa, *J. Chem. Phys.*, 2009, **130**, 214506.
35 H. Staleva, M. Zeeshan, P. Chábera, V. Partali, H. R. Sliwka and T. Polívka, *J. Phys. Chem. A*, 2015, **119**, 11304.
36 D. M. Niedzwiedzki, T. Kajikawa, K. Aoki, S. Katsumura and H. A. Frank, *J. Chem. Phys. B*, 2013, **117**, 6874–6887.
37 D. Kosumi, T. Kajikawa, S. Okumura, M. Sugisaki, K. Sakaguchi, S. Katsumura and H. Hashimoto, *J. Phys. Chem. Lett.*, 2014, **5**, 792–797.
38 T. Kajikawa, K. Aoki, R. S. Singh, T. Iwashita, T. Kusumoto, H. A. Frank, H. Hashimoto and S. Katsumura, *Org. Biomol. Chem.*, 2009, **7**, 3723–3733.
39 D. Kosumi, T. Kajikawa, K. Yano, S. Okumura, M. Sugisaki, K. Sakaguchi, S. Katsumura and H. Hashimoto, *Chem. Phys. Lett.*, 2014, **602**, 75–79.
40 M. M. Enriquez, S. Hananoki, S. Hasegawa, T. Kajikawa, S. Katsumura, N. L. Wagner, R. R. Birge and H. A. Frank, *J. Phys. Chem. B*, 2012, **116**, 10748–10756.
41 H.-R. Sliwka and V. Partali, *Molecules*, 2012, **17**, 2877–2928.
42 M. P. O'Neil, M. R. Wasielewski, M. M. Khaled and L. D. Kispert, *J. Chem. Phys.*, 1991, **95**, 7212–7218.
43 P. Chábera, M. Fuciman, K. Razi Naqvi and T. Polívka, *Chem. Phys.*, 2010, **373**, 56–64.
44 H. Fukami, K. Namikawa, N. Sugiura-Tomimori, M. Sumida, K. Katano and M. Nakao, *J. Oleo Sci.*, 2006, **55**, 653–656.
45 H. L. Jackson, A. J. Cardounel, J. L. Zweier and S. F. Lockwood, *Bioorg. Med. Chem. Lett.*, 2004, **14**, 3985–3991.
46 J. Willibald, S. Rennebaum, S. Breukers, S. H. Abdel Hafez, A. Patel, C. L. Øpstad, R. Schmid, S. N. Naess, H.-R. Sliwka and V. Partali, *Chem. Phys. Lipids*, 2009, **161**, 32–37.
47 R. Litvín, D. Bína, M. Herbstová and Z. Gardian, *Photosynth. Res.*, 2016, **130**, 137–150.
48 I. F. Sengul, K. Wood, N. Kumar and D. S. Black, *Tetrahedron*, 2012, **68**, 9050–9055.
49 K. Holtin, M. Kuehnle, J. Rehbein, P. Schuler, G. Nicholson and K. Albert, *Anal. Bioanal. Chem.*, 2009, **395**, 1613–1622.
50 J. Kevin, H. Stapelfeldt and L. H. Skibsted, *Chem. Phys. Lett.*, 1992, **190**, 514–519.
51 T. Khan, R. Litvín, V. Šebelík and T. Polívka, *ChemPhysChem*, 2021, **22**, 471–480.
52 M. Fuciman, M. Durchan, V. Slouf, G. Kesan and T. Polivka, *Chem. Phys. Lett.*, 2013, **568**, 21–25.
53 M. Fuciman, G. Kesan, A. M. LaFountain, H. A. Frank and T. Polivka, *J. Phys. Chem. B*, 2015, **119**, 1457–1467.
54 H. Hashimoto, T. Yoda, T. Kobayashi and A. J. Young, *J. Mol. Struct.*, 2002, **604**, 125–146.
55 H. Staleva-Musto, V. Kuznetsova, D. Bína, R. Litvín and T. Polívka, *Photosynth. Res.*, 2020, **144**, 127–135.

